Research Article Vol. 33, No. 2 / 27 Jan 2025 / Optics Express 2620
Optics EXPRESS

All-polarization-maintaining dual-comb Er-fiber laser with combined figure-8 and figure-9 architectures

WEI-TING LIN,[1] YUAN-TING LIU,[2] ZHI-MING HSIEH,[2] CHING-MING CHEN,[2] HSUN HSU,[2] JIN-LONG PENG,[3] WEI-WEI HSIANG,[2,*] AND RAY-KUNG LEE[1,4,5,6]

[1]*Department of Physics, National Tsing Hua University, Hsinchu 30013, Taiwan*
[2]*Department of Physics, Fu Jen Catholic University, New Taipei City 24205, Taiwan*
[3]*Center for Measurement Standards, Industrial Technology Research Institute, Hsinchu 30011, Taiwan*
[4]*Institute of Photonics Technologies, National Tsing Hua University, Hsinchu 30013, Taiwan*
[5]*Center for Theory and Computation, National Tsing Hua University, Hsinchu 30013, Taiwan*
[6]*Center for Quantum Science and Technology, Hsinchu 30013, Taiwan*
[*]*069179@mail.fju.edu.tw*

Abstract: We propose and demonstrate, for the first time to the best of our knowledge, an all-polarization-maintaining (all-PM) dual-comb Er-fiber laser based on combined figure-8 and figure-9 architectures. The opposite signs of the non-reciprocal phase shifts required for figure-8 and figure-9 architectures in the shared nonlinear amplifying loop mirror (NALM) are achieved using a single non-reciprocal phase shifter (NRPS) that operates in two orthogonal polarizations. The capability of common mode noise cancellation, environmental stability, long-term reliability, and the tunable range of the repetition rate difference Δf_{rep} between two combs has been investigated and characterized. In addition, the dual-comb spectroscopy measurement with our dual-comb fiber laser is demonstrated to resolve the transmission spectrum of a flat-top DWDM (dense wavelength division multiplexer) demultiplexer, with a passband of ~50 GHz at 1564.5 nm. Our experimental results indicate that the combined-architecture all-PM fiber laser, with its large tunable range of 100 kHz in Δf_{rep}, shows significant potential for dual-comb applications in precise and rapid metrology outside the laboratory.

1. Introduction

Precise, rapid, and sensitive measurements based on dual-comb techniques have been successfully developed in a variety of schemes and gained significant improvements in metrology, including dual-comb spectroscopy [1–7], dual-comb ranging [7–15], and other new characterization methods using asynchronous optical sampling [16–21]. In the time domain, the light sources employed in the dual-comb techniques are two different periodic ultrashort optical pulse trains with a small repetition rate difference Δf_{rep}. One pulse train with the repetition rate f_{rep1}, is utilized to probe the sample or to measure the distance, while the other with a slightly different repetition rate $f_{rep2} = f_{rep1} + \Delta f_{rep}$ is used to asynchronously sample the probe pulses to extract the measured information, which shows an interferogram with a repeating rate of Δf_{rep}. In the frequency domain, the dual-comb light sources are two optical frequency combs with different line spacings. The slightly different line spacing Δf_{rep} of the dual-comb facilitates multi-heterodyne detection, allowing the information encoded in each line of the first optical comb to be down-converted to the radio-frequency (RF) domain through heterodyning with the second optical comb, which acts as the local oscillator. The Fourier transformation of the interferogram in time domain corresponds to the heterodyne beat frequency in the frequency domain. Therefore, dual-comb techniques enable optical measurements to be more rapid and precise by directly accessing fast

#544280 https://doi.org/10.1364/OE.544280
Journal © 2025 Received 11 Oct 2024; revised 25 Dec 2024; accepted 30 Dec 2024; published 17 Jan 2025

Optics EXPRESS

RF electronics to process the signals of interferograms or cross-correlations. On the other hand, timing or frequency parameters of the dual-comb, i.e., the individual repetition rates and the repetition rate difference, also determine the measurement limits in dual-comb applications. For instance, the tradeoff between the acquisition rate Δf_{rep} and the non-aliasing optical bandwidth, which is inversely proportional to Δf_{rep}, must be considered when deploying the light sources used in dual-comb spectroscopy [1]. For dual-comb ranging/LiDAR applications, the updated rate is the repetition rate difference Δf_{rep}, while the unambiguous range is inversely proportional to Δf_{rep} when exploiting the Vernier effect [8,9,13].

In conventional dual-comb techniques, two independent mode-locked lasers are phase-locked to a highly frequency-stable continuous wave laser using a delicate servo system to maintain mutual coherence. This approach is bulky, complex, and expensive. Recently, single-cavity mode-locked lasers have proven to be promising for various applications of dual-comb measurements due to their ability to passively suppress common-mode noises [13,20–35]. Among these, single-cavity dual-comb fiber lasers offer advantages in simplicity, compactness, robustness, and low cost [20–35]. These dual-comb fiber lasers have been demonstrated using various multiplexing techniques, including wavelength multiplexing, polarization multiplexing, and bi-directional configurations. In particular, bidirectional single-cavity fiber lasers have been shown to significantly reduce the impact of pulse collision effects in the dual-comb due to their counter-propagation configuration [25–27]. However, it is still desirable to develop the all-polarization-maintaining (all-PM) dual-comb fiber laser based on the nonlinear amplifying loop mirror (NALM) [28–30,33,34,36]. These NALM-based fiber lasers exhibit superior features in environmental stability and long-term reliability, which are crucial for fieldable dual-comb applications in precise and rapid metrology outside the laboratory.

Here we propose and demonstrate, for the first time to our best knowledge, the tunable dual-comb from an all-PM Er-fiber laser based on combined figure-8 and figure-9 architectures with a shared NALM. For two orthogonal polarizations, a single non-reciprocal phase shifter (NRPS) in the shared NALM can simultaneously provide the necessary nonreciprocal phase shifts with opposite signs for the figure-8 and figure-9 architectures [36]. Previous fiber lasers with a dual figure-9 configuration require tuning two independent NRPSs located on the non-shared paths to obtain the required phase shift [30,33,34] for mode-locking the dual-comb laser. Environmental perturbation on these NRPSs may introduce uncancelled noises. Our novel design using a single common NRPS eliminates this possibility and simplifies the construction of NALM-based dual-comb fiber laser. Additionally, the combined-cavity structure also allows for a larger repetition rate difference in the dual comb compared to single-cavity fiber lasers, where birefringence or dispersion effects typically limit the maximum repetition rate difference to only a few kHz [28,29].

Although such an NALM-based dual-comb fiber laser with a combined cavity offers features such as environmental immunity, long-term reliability, and spectral overlap, the crucial ability of common-mode noise cancellation for different values of the repetition rate difference Δf_{rep} has not yet been experimentally investigated in Refs. [30,33,34]. In this study, nearly 60% of the total cavity length of the figure-8 or figure-9 architectures overlaps, and the impact of pulse collisions on stability has been experimentally examined as the repetition rate is varied from 100 kHz to ~1 kHz. When the repetition rate is reduced to 1.6 kHz, both stable and bistable dual-comb dynamics are observed. On one hand, the observation of bistable dual-comb dynamics suggests that our combined-cavity fiber laser could serve as a new platform for studying new complex pulse interactions in dissipative nonlinear systems [24,37,38]. On the other hand, under stable dual-comb dynamics, our dual-comb fiber laser has been demonstrated to perform dual-comb spectroscopy, successfully resolving the transmission spectrum of a flat-top DWDM (dense wavelength division multiplexer) demultiplexer, with a passband of ~50 GHz at 1564.5 nm. Our experimental results indicate that this combined-architecture all-PM fiber laser, with a large

Optics EXPRESS

tunable range in Δf_{rep}, shows great potential for dual-comb applications in precise and rapid metrology outside the laboratory.

2. Experimental setup of the combined figure-8 and figure-9 architectures

Figure 1 shows the schematic of the all-PM Er-fiber laser based on combined figure-8 (F8) and figure-9 (F9) architectures [36]. The shared NALM consists of a 50/50 fiber coupler, a wavelength-division multiplexing (WDM) fiber coupler, 50-cm long Er-doped fiber (LIEKKI, Er80-4/125-HD-PM), a 976-nm pump laser diode, and a NRPS. All the PM fiber devices in the shared NALM can work for both slow and fast axes of the PM fiber. The commercial NRPS (Haphit Ltd.) in the shared NALM consists of a quarter-wave plate (QWP) and two Faraday rotators with opposite rotation directions. As shown in Fig. 1, the orientations of the principal axes of the QWP, labeled as x' and y', are rotated 45 degrees relative to the slow and fast axes of the PM fibers, denoted as x and y. For two orthogonal polarizations along x and y axes, the signs of the phase shift differences between the lights passing the NRPS in clockwise and counterclockwise directions are opposite, i.e., $\pi/2$ and $-\pi/2$. Therefore, a single NRPS that simultaneously provides two opposite nonreciprocal phase shifts enables mode-locking in both figure-8 and figure-9 architectures through polarization multiplexing. Using a fused-fiber polarization splitter/combiner (FFBS/C), the light circulating in the shared NALM with polarization along the slow axis is connected to the linear arm of the figure-9 architecture, while the light polarized along the fast axis is routed to the transmission loop of the figure-8 architecture. Compared to other single-cavity fiber lasers, these two separate sections enable wider and more flexible tuning of the dual-comb. In the linear arm of the figure-9 architecture, a cube polarization beam splitter (PBS) is used to ensure the light to be polarized along the slow axis. The output of the figure-9 mode-locking is delivered through the partial reflector (10% transmission) and an optical isolator. In the transmission loop of the figure-8 architecture, an optical isolator ensures unidirectional propagation while maintaining polarization along the fast axis. Two crossed fiber splices exchange polarization between the fast and slow axes as the light passes through the

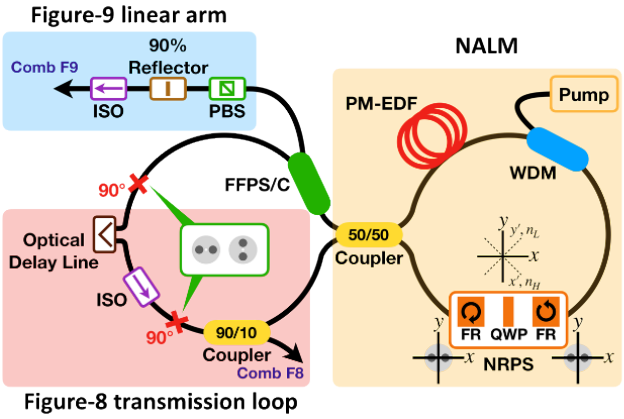

Fig. 1. The schematic of the experimental setup of the dual-comb all-PM Er-fiber laser with combined figure-8 and figure-9 architectures. F8, figure-8; F9, figure-9; NALM, nonlinear amplifying loop mirror; NRPS, non-reciprocal phase shifter; FR, Faraday rotator; QWP, quarter-wave plate; x and y, slow and fast axes of the PM fiber; x' and y', slow and fast axes of the QWP; n_H and n_L, refractive indices of slow and fast axes of the QWP; WDM, 976/1560 nm wavelength division multiplexer; PM-EDF, polarization-maintaining Er-doped fiber; FFPS/C, fused-fiber polarization splitter/combiner; PBS, polarization beam splitter; ISO, optical isolator; Pump, 976-nm laser diode.

Optics EXPRESS

slow-axis-working optical isolator. The output of the figure-8 mode-locking is obtained from a 90/10 fiber coupler. Additionally, an optical delay line with a maximum tunable range of 500 ps is included to adjust the cavity length of the figure-8 architecture. Therefore, the wide tunable range of the repetition rate difference between the figure-8 and figure-9 combs can be achieved. The shared section of the cavity, including the common NALM and the input fiber of the FFBS/C, is approximately 6.5-m long, which accounts for nearly 60% of the total cavity length of the figure-8 or figure-9 architecture. To the best of our knowledge, this is the first time that combined figure-8 and figure-9 architectures with a shared NALM, utilizing polarization multiplexing through a single NRPS, have been used to construct a dual-comb all-PM Er-fiber laser.

3. Experimental results

3.1. Dual-comb mode-locking with tunable repetition rate differences

For dual-comb operation, we observed that the self-starting capability of mode-locking in typical NALM-based fiber lasers with the NRPS cannot be obtained in our combined figure-8 and figure-9 architectures. However, it was found that dual-comb mode-locking can be easily initialized by slightly perturbing the fiber of the linear arm in the figure-9 architecture with a pump power of approximately 400 mW. The multiple-pulse mode-locking was initially observed and can be transferred to the single-pulse mode-locking by reducing the pump power approximately down to range of 120 mW to 100 mW. Figure 2(a) shows the optical spectra measured from the two outputs of the all-PM dual-comb Er-fiber laser. The center wavelength of the comb figure-8 (comb F8) is 1564 nm, with a full-width half-maximum (FWHM) optical bandwidth of 6.5 nm. The center wavelength of the comb figure-9 (comb F9) is 1566 nm, with an FWHM optical bandwidth of 9.2 nm. The overlapped optical spectra of the comb F8 and the comb F9 significantly facilitates the following two-comb applications. Since both the net cavity dispersions of the figure-8 and figure-9 structures are anomalous, intriguing phenomena of sidebands in the optical spectra, resulting from constructive or destructive interference between the soliton and dispersive waves, can be observed in these mode-locked soliton fiber lasers [39–41]. The oscilloscope traces and the RF spectra of the pulse trains, as shown in Fig. 2(b) and 2(c), indicate that the repetition rates of comb F8 and comb F9 are approximately 19.57 MHz. The average power from the outputs of comb F8 and comb F9 is measured to be 0.96 mW and 0.85 mW, respectively, with the shared NALM at a pump power of approximately 110 mW.

Figure 3 shows the tuning of the repetition rate difference of the dual-comb, ranging from 100 kHz to 1.6 kHz. The repetition frequency of comb F9 is fixed, while the repetition rate of comb F8 is adjusted to vary the repetition rate difference using the optical delay line. The upper limit of the repetition rate difference depends on the tunable range of the optical delay line, which is greater than 100 kHz in our experiment. When the repetition rate difference is less than $\sim$ 1 kHz, stable dual-comb mode-locking fails to be maintained due to unavoidable pulse collisions in our combined figure-8 and figure-9 architectures. Figures 3(a), (c), and (e) show the RF spectra measured from the output of comb F8 when the repetition rate difference is adjusted to 100 kHz, 10 kHz, and 1.6 kHz, respectively. The corresponding RF spectra measured from the output of comb F9 are shown in Figs. 3(b), (d), and (f). The crosstalk between comb F8 and comb F9 can be observed due to the limited polarization extinction ratios (PER) of the FFPS/C and other PM fiber devices. Thanks to the long-term robustness and environmental stability of all-PM NALM-based fiber lasers, dual-comb mode-locking can be maintained for weeks during our long-term characterization experiments.

3.2. Temporal variations of the dual-comb for Δf_{rep} of 100 kHz and 10 kHz

To investigate the ability to cancel common-mode noise, the repetition rates of comb F8 and comb F9 were measured simultaneously using two connected frequency counters (Keysight

Optics EXPRESS

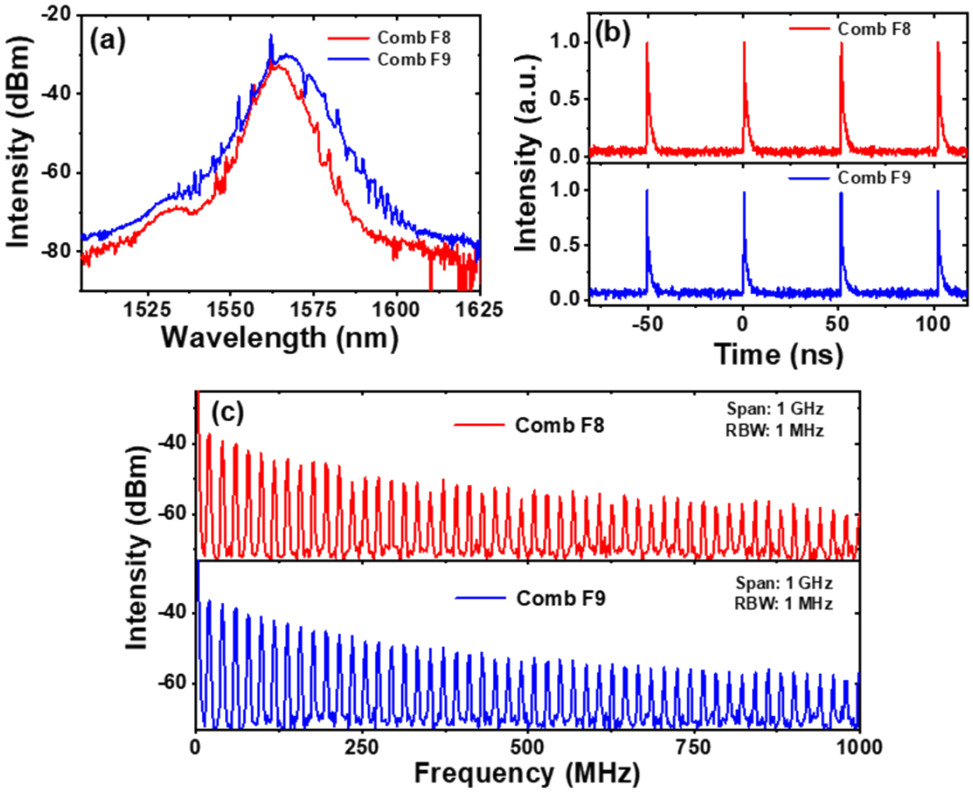

Fig. 2. (a) Optical spectra, (b) oscilloscope traces, and (c) RF spectra of comb F8 (red) and comb F9 (blue) measured from two outputs respectively of the dual-comb Er-fiber laser.

53220A) with a gate time of 1 second. Figure 4(a) and 4(b) show the temporal variations when the repetition rate difference is 100 kHz, recorded over a period of 10,000 s. The repetition rates of the comb F8 and comb F9 are ~19.476 MHz and ~19.576 MHz, and the corresponding repetition rate difference is 100 kHz. The deviations of the repetition rates for comb F8 and comb F9 are 6.36 Hz and 6.57 Hz, respectively, while the deviation of the repetition rate difference is 0.33 Hz, which is significantly smaller than those of the individual repetition rates. This clearly indicates that the combined figure-8 and figure-9 architectures with the shared NALM can effectively suppress common-mode noise. The calculated Allan deviation of the repetition rate difference is shown in Fig. 4(c). For the integration time ranging from 1 s to 10 s, the Allan deviation remains nearly constant. However, for the integration time from 50 s to 1000 s, the Allan deviation varies with the integration time with a slope of $\tau^{0.75}$, which is larger than the slope of $\tau^{0.5}$ for the random walk [27]. These observations show that, on one hand, short-term common-mode noise can be effectively suppressed owing to the shared NALM. On the other hand, long-term drifts are not perfectly canceled due to the incomplete overlap of the combined figure-8 and figure-9 architectures. The same measurement was performed when the repetition rate difference was reduced to 10.2 kHz, as shown in Figs. 5(a) and (b). The deviations of the repetition rates for comb F8 and comb F9 are 21.30 Hz and 21.31 Hz, respectively, while the deviation of the repetition rate difference is 0.27 Hz. Figure 5(c) shows the behavior of the Allan deviation for Δf_{rep} at 10 kHz is similar to that at 100 kHz, except for a slightly larger deviation near the integration time of 10 seconds. The reason for the increased deviation may result from

Optics EXPRESS

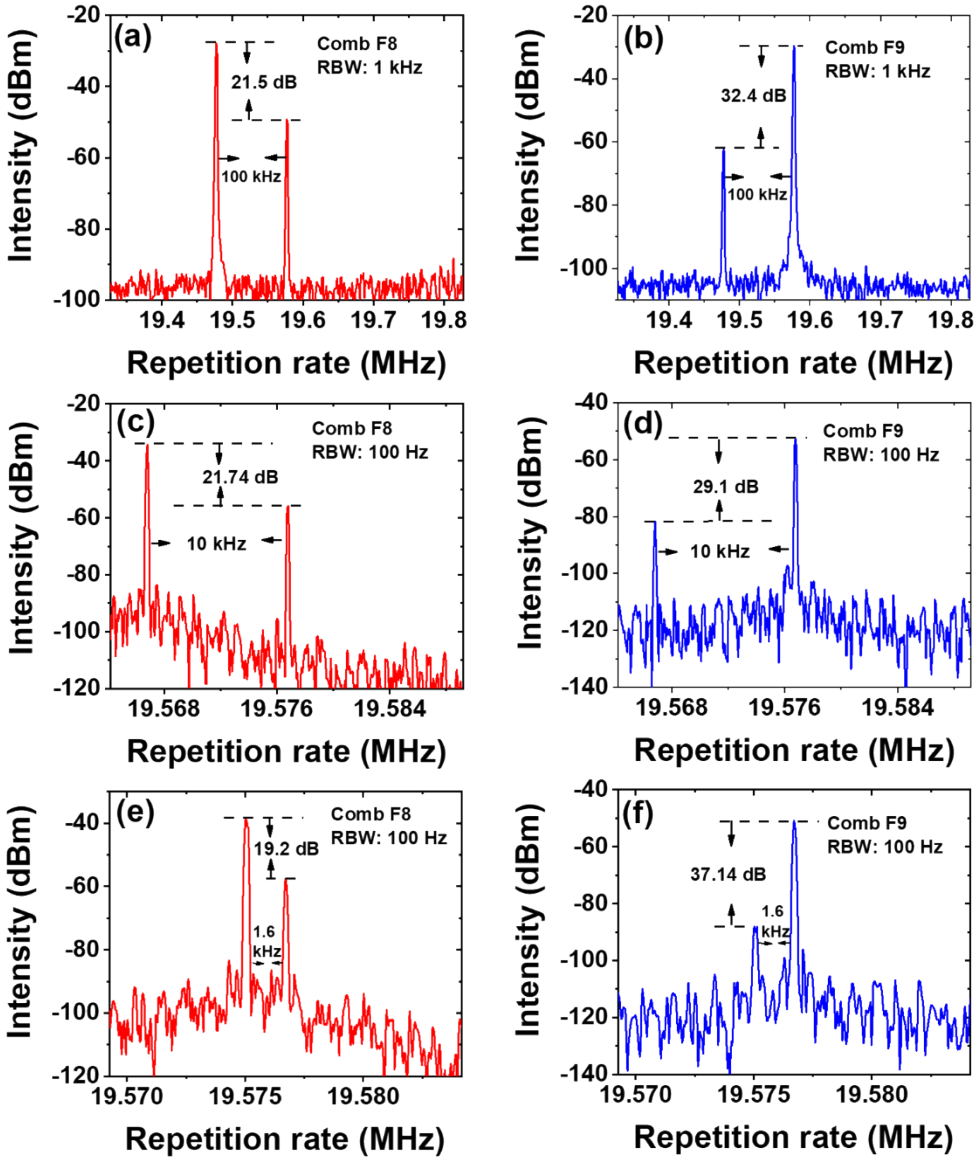

Fig. 3. RF spectra measured form the outputs of comb F8 (red) and comb F9 (blue), respectively. The repetition frequency difference is varied to (a-b) 100 kHz, (c-d) 10 kHz, and (e-f) 1.6 kHz. RBW, the resolution bandwidth of the RF spectrum analyzer.

the effect of pulse collisions, which become more significant as the repetition rate difference decreases [24,28].

3.3. *Dual-comb dynamics when Δf_{rep} =1.6 kHz*

When the repetition rate difference Δf_{rep} decreases to a few kHz, two types of distinct dual-comb dynamics are observed. Figure 6 (a) shows the measurement results over a period of 40000 s when the repetition rate difference is ~1.6 kHz. In addition to the stable dual-comb dynamics, as presented in Sec. 3.2, oscillatory phenomena in Δf_{rep} have also been observed. Between t =20000 s and t =40000 s (e.g., $t = t_5$), the deviation of Δf_{rep} is only 0.23 Hz, while Δf_{rep}

Optics EXPRESS

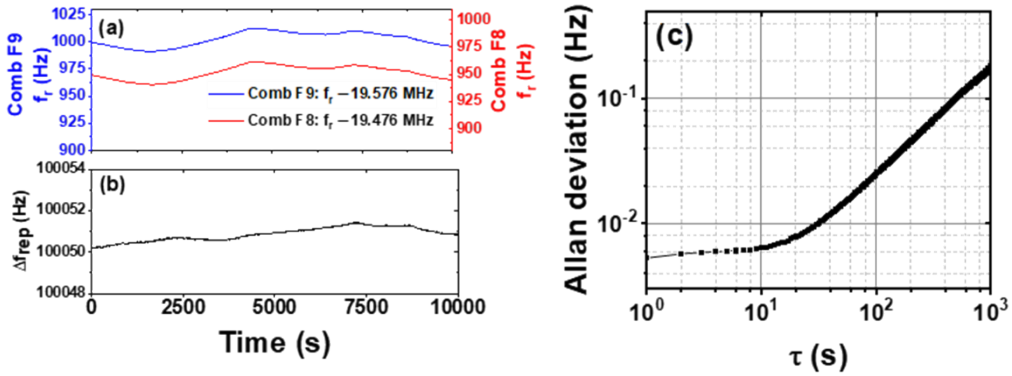

Fig. 4. The measurement of temporal variations when the repetition rate difference is 100 kHz. (a) The individual repetition rates (red: comb F8, blue: comb F9). (b) The repetition rate difference. (c) The corresponding calculated Allan deviations.

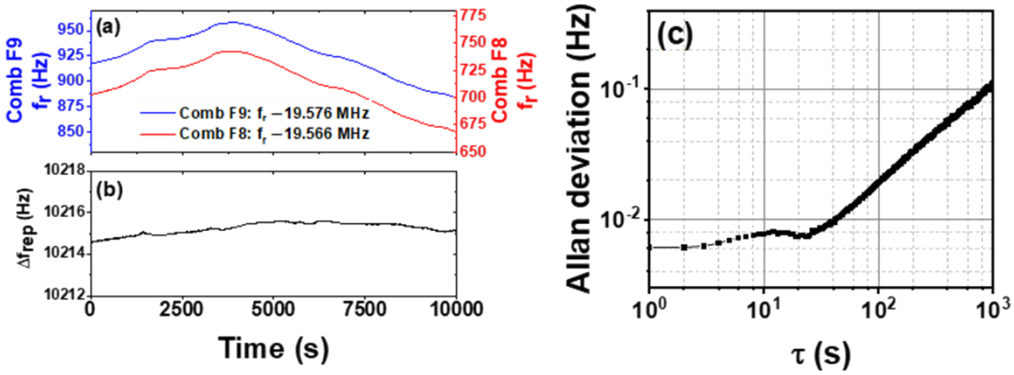

Fig. 5. The measurement of temporal variations when the repetition rate difference is 10 kHz. (a) The individual repetition rates (red: comb F8, blue: comb F9). (b) The repetition rate difference. (c) The corresponding calculated Allan deviations.

oscillates between 1620 Hz and 1660 Hz between t =0 and t =20000 s. Furthermore, it is found that the oscillations are a result of the much larger variation in the comb F9 so that the oscillations cannot be effectively canceled by the comb F8. To clarify the underlying mechanisms responsible for the oscillation in the dual-comb dynamics, the optical spectrum of comb F9 is measured simultaneously with the repetition rates. It is worth noting that the changes in the repetition rate are always accompanied by variations in the optical spectrum. As shown in Fig. 6(b) and 6(c), there is a blue shift in the optical spectrum at time t_1 =14066 s compared to that at time t_2 =15128 s. Such a blue shift will cause the pulse to speed up due to the net anomalous dispersion of the cavity. Consequently, the repetition rate of comb F9 will also increase. A similar observation was noted when comparing the optical spectra measured at time t_3 =18048 s and time t_4 =18845 s, as shown in Fig. 6(b) and 6(d). The red shift in the optical spectrum will cause the pulse to slow down, leading to a decrease in the repetition rate of comb F9. The above observations reveal that the oscillations or instabilities in the dual-comb dynamics are caused by the collision-induced frequency shift resulting from the nonlinear effect of cross-phase modulation in the PM fiber [24,42–44]. It is worth noting that previous studies have reported that the effects from this pulse collision dissipate completely before the subsequent collision takes place [24,28]. In contrast to other fiber lasers based on unidirectional single-cavity structures, our combined-cavity fiber

Optics EXPRESS

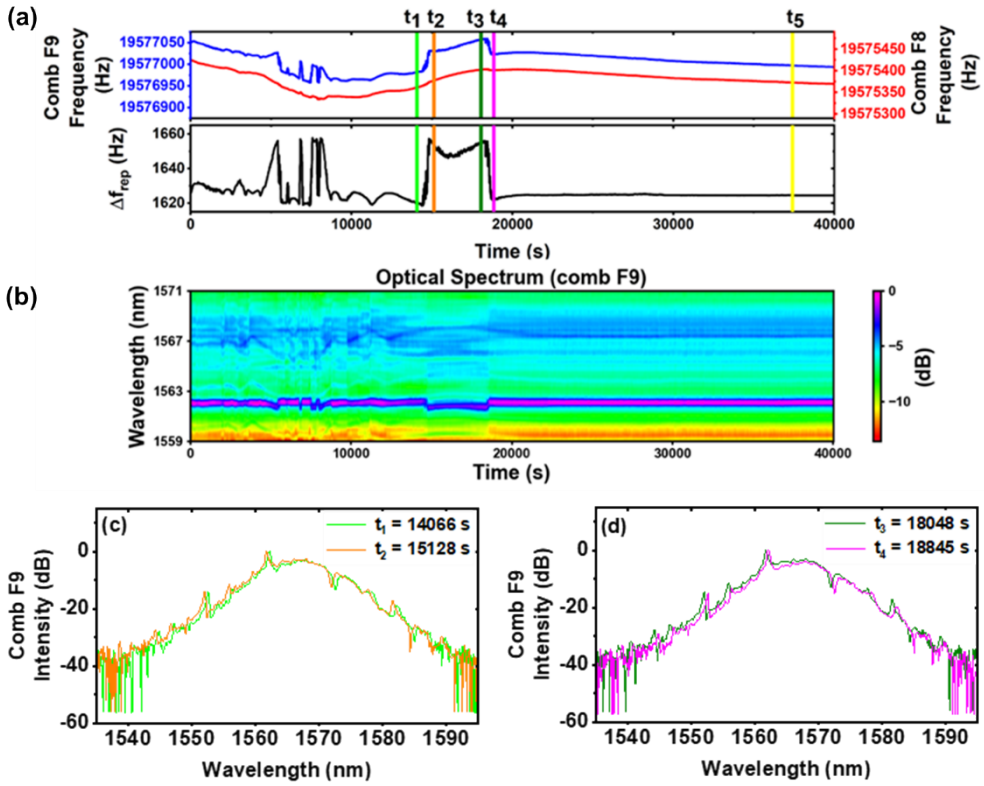

Fig. 6. The measurement of temporal variations when the repetition rate difference is ~1.6 kHz. (a) The individual repetition rates (red: comb F8, blue: comb F9) and the repetition rate difference. (b) The partial optical spectrum, only shown between 1559 nm and 1571 nm, of comb F9. (c) and (d) The entire optical spectra of comb F9 measured at different times.

laser can experience not only complete pulse collisions but also partial collisions between the pulses. The difference in group velocities between the two polarizations along the fast and slow axes of the PM fiber is measured to be 1.4 ps/m, with an estimated birefringent walk-off length of 0.35 m. Partial collisions will occur when the pulses from the figure-8 loop and the figure-9 linear branch return and coincide at the 50/50 fiber coupler of the shared NALM. The effects of pulse collisions in birefringent optical fibers have been extensively studied, and it is known that partial collisions have much stronger effects than those resulting from complete collisions [42–44]. This could act as the critical mechanism for triggering oscillations in the dual-comb dynamics of the combined figure-8 and figure-9 structures, particularly as the repetition rate difference approaches just a few kHz.

Optics EXPRESS

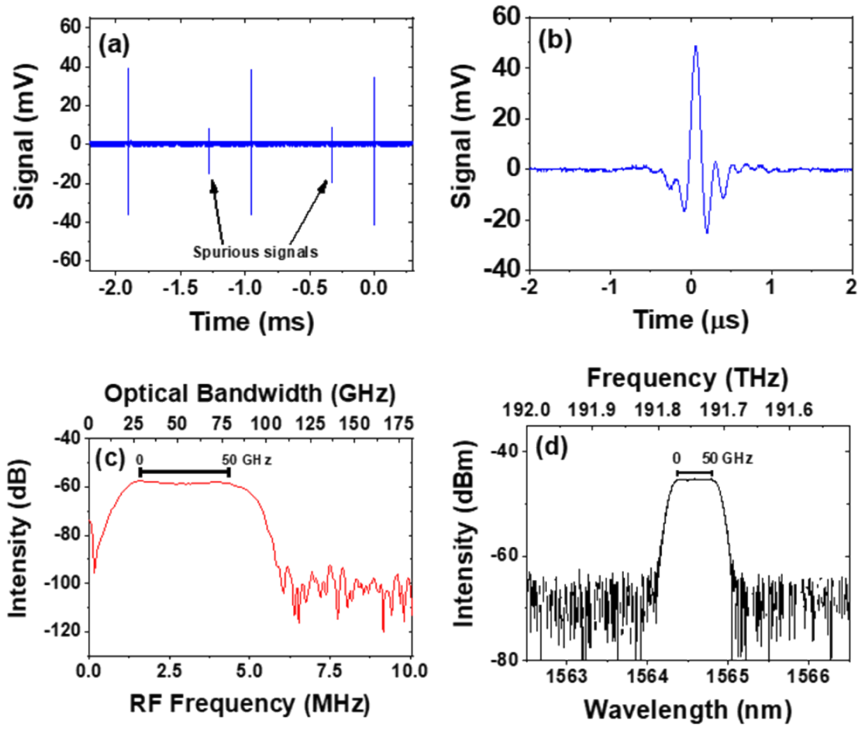

Fig. 7. The measurement of transmission spectrum of a DWDM demultiplexer. (a) A series of the dual-comb interferograms with a period of 0.91 ms. (b) and (c) One of the magnified interferogram and its RF spectrum obtained using fast Fourier transform (FFT). (d) The optical spectrum measured with an optical spectrum analyzer.

4. Measurement of transmission spectrum of a DWDM demultiplexer

To demonstrate its capability in metrology applications, we employed our dual-comb fiber laser to measure the transmission spectrum of a DWDM (dense wavelength division multiplexing) demultiplexer, which features a flat-top passband of ~50 GHz at 1564.5 nm. In this dual-comb spectroscopy measurement, the repetition rate difference between comb F8 and comb F9 was finely tuned to 1.1 kHz, resulting in a non-aliasing optical bandwidth of 174 GHz. The outputs of comb F8 and comb F9 were firstly combined using a 50/50 fiber coupler, and one output port of the 50/50 fiber coupler was connected to the DWDM demultiplexer. After passing the DWDM demultiplexer, the light was measured with a photodetector. The electric signal of the photodetector was processed with a RF lowpass filter of 5 MHz and measured by a digital oscilloscope. As shown in Fig. 7(a), a series of the interferograms were repeated every 0.91 ms. In Fig. 7(a), in addition to the interferogram of the dual-comb, the spurious signals appear due to intra-cavity cross-talk, which arises from pulse collisions within the cavity and leads to amplitude modulation on both figure-8 and figure-9 pulse trains [28]. Figure 7(b) and 7(c) displays one of the interferograms and its RF spectrum obtained using fast Fourier transform (FFT). The RF spectrum reveals a flat-top transmission profile with a passband of 2.83 MHz, corresponding to a 50.4 GHz optical bandwidth for our dual-comb system. This result is consistent with Fig. 7(d), which was measured using an optical spectrum analyzer. This clearly demonstrates the ability of our dual-comb system to resolve the spectral features of the DWDM demultiplexer and highlights its potential for various metrology applications. To further improve our dual-comb system for practical applications, the overlap between the F8 and F9 configurations should be increased.

Optics EXPRESS

This can be achieved by reducing the length of the F8 transmission loop (or twice the length of the F9 linear arm). Additionally, measuring the carrier-envelope frequencies of our dual-comb fiber is an interesting direction for future research [26].

5. Conclusions

For the first time to our best knowledge, a dual-comb all-PM Er-fiber laser based on combined figure-8 and figure-9 architectures with a shared NALM, utilizing polarization multiplexing through a single NRPS, has been proposed and demonstrated. The shared NALM plays a crucial role in suppressing common-mode noises in the dual-comb system, while the non-overlapping parts of the cavity provide flexibility in tuning the repetition rate difference Δf_{rep} from 100 kHz to approximately 1 kHz. As the repetition rate difference Δf_{rep} is reduced to a few kHz, an intriguing feature of the oscillation in Δf_{rep} has been observed, potentially arising from pulse collisions in our combined fiber laser cavity. Our experimental results show that this environmentally stable and long-term reliable all-PM dual-comb fiber laser, with a wide tunable range in Δf_{rep}, has significant potential for practical dual-comb applications in precise and rapid metrology outside the laboratory.

Funding. National Science and Technology Council, Taiwan (No. 108-2119-M-030-001-MY2, No. 112-2123-M-007-001, No. 112-2119-M-008-007, No. 112-2119- M-007-006).

Disclosures. The authors declare no conflicts of interest.

Data availability. Data underlying the results presented in this paper are not publicly available at this time but may be obtained from the authors upon reasonable request.

References

1. I. Coddington, N. Newbury, and W. Swann, "Dual-comb spectroscopy," Optica **3**(4), 414–426 (2016).
2. N. Picqué and T. W. Hänsch, "Frequency comb spectroscopy," Nat. Photonics **13**(3), 146–157 (2019).
3. S. Schiller, "Spectrometry with frequency combs," Opt. Lett. **27**(9), 766–768 (2002).
4. F. Keilmann, C. Gohle, and R. Holzwarth, "Time-domain mid-infrared frequency-comb spectrometer," Opt. Lett. **29**(13), 1542–1544 (2004).
5. A. Schliesser, M. Brehm, F. Keilmann, *et al.*, "Frequency-comb infrared spectrometer for rapid, remote chemical sensing," Opt. Express **13**(22), 9029–9038 (2005).
6. I. Coddington, W. C. Swann, and N. R. Newbury, "Coherent multiheterodyne spectroscopy using stabilized optical frequency combs," Phys. Rev. Lett. **100**(1), 013902 (2008).
7. T. Fortier and E. Baumann, "20 years of developments in optical frequency comb technology and applications," Commun. Phys. **2**(1), 153 (2019).
8. I. Coddington, W. C. Swann, L. Nenadovic, *et al.*, "Rapid and precise absolute distance measurements at long range," Nat. Photonics **3**(6), 351–356 (2009).
9. Z. Zhu and G. Wu, "Dual-comb ranging," Engineering **4**(6), 772–778 (2018).
10. H. Zhang, H. Wei, X. Wu, *et al.*, "Absolute distance measurement by dual-comb nonlinear asynchronous optical sampling," Opt. Express **22**(6), 6597–6604 (2014).
11. G. Wu, S. Xiong, K. Ni, *et al.*, "Parameter optimization of a dual-comb ranging system by using a numerical simulation method," Opt. Express **23**(25), 32044–32053 (2015).
12. J. Riemensberger, A. Lukashchuk, M. Karpov, *et al.*, "Massively parallel coherent laser ranging using a soliton microcomb," Nature **581**(7807), 164–170 (2020).
13. S. L. Camenzind, J. F. Fricke, J. Kellner, *et al.*, "Dynamic and precise long-distance ranging using a free-running dual-comb laser," Opt. Express **30**(21), 37245–37260 (2022).
14. J. Fellinger, G. Winkler, P. E. C. Aldia, *et al.*, "Simple approach for extending the ambiguity-free range of dual-comb ranging," Opt. Lett. **46**(15), 3677–3680 (2021).
15. H. Wright, A. J. M. Nelmes, N. J. Weston, *et al.*, "Multi-target two-photon dual-comb LiDAR," Opt. Express **31**(14), 22497–22506 (2023).
16. A. Asahara and K. Minoshima, "Development of ultrafast time-resolved dual-comb spectroscopy," APL Photonics **2**(4), 041301 (2017).
17. A. Asahara, Y. Arai, T. Saito, *et al.*, "Dual-comb-based asynchronous pump-probe measurement with an ultrawide temporal dynamic range for characterization of photo-excited InAs quantum dots," Appl. Phys. Express **13**(6), 062003 (2020).
18. T. Mizuno, Y. Nakajima, Y. Hata, *et al.*, "Computationally image-corrected dual-comb microscopy with a free-running single-cavity dual-comb fiber laser," Opt. Express **29**(4), 5018–5032 (2021).

Optics EXPRESS

19. X. Dong, X. Zhou, J. Kang, *et al.*, "Ultrafast time-stretch microscopy based on dual-comb asynchronous optical sampling," Opt. Lett. **43**(9), 2118–2121 (2018).
20. X. Zhao, Z. Zheng, L. Liu, *et al.*, "Fast, long-scan-range pump-probe measurement based on asynchronous sampling using a dual-wavelength mode-locked fiber laser," Opt. Express **20**(23), 25584–25589 (2012).
21. G. Hu, T. Mizuguchi, X. Zhao, *et al.*, "Measurement of absolute frequency of continuous-wave terahertz radiation in real time using a free-running, dual-wavelength mode-locked, erbium-doped fibre laser," Sci. Rep. **7**(1), 42082 (2017).
22. X. Zhao, Z. Zheng, L. Liu, *et al.*, "Switchable, dual-wavelength passively mode-locked ultrafast fiber laser based on a single-wall carbon nanotube modelocker and intracavity loss tuning," Opt. Express **19**(2), 1168–1173 (2011).
23. L. Yun, X. Liu, and D. Mao, "Observation of dual-wavelength dissipative solitons in a figure-eight erbium-doped fiber laser," Opt. Express **20**(19), 20992–20997 (2012).
24. Y. Wei, B. Li, X. Wei, *et al.*, "Ultrafast spectral dynamics of dual-color-soliton intracavity collision in a mode-locked fiber laser," Appl. Phys. Lett. **112**(8), 081104 (2018).
25. X. Zhao, Z. Zheng, Y. Liu, *et al.*, "Dual-wavelength, bidirectional single-wall carbon nanotube mode-locked fiber laser," IEEE Photonics Technol. Lett. **26**(17), 1722–1725 (2014).
26. Y. Nakajima, Y. Hata, and K. Minoshima, "High-coherence ultra-broadband bidirectional dual-comb fiber laser," Opt. Express **27**, 5931–5944 (2019).
27. B. Li, J. Xing, D. Kwon, *et al.*, "Bidirectional mode-locked all-normal dispersion fiber laser," Optica **7**(8), 961–964 (2020).
28. J. Fellinger, A. S. Mayer, G. Winkler, *et al.*, "Tunable dual-comb from an all-polarization-maintaining single-cavity dual-color Yb:fiber laser," Opt. Express **27**(20), 28062–28074 (2019).
29. R. Li, H. Shi, H. Tian, *et al.*, "All-polarization-maintaining dual-wavelength mode-locked fiber laser based on Sagnac loop filter," Opt. Express **26**(22), 28302–28311 (2018).
30. Y. Nakajima, Y. Hata, and K. Minoshima, "All-polarization-maintaining, polarization-multiplexed, dual-comb fiber laser with a nonlinear amplifying loop mirror," Opt. Express **27**(10), 14648–14656 (2019).
31. X. Zhao, T. Li, Y. Liu, *et al.*, "Polarization-multiplexed, dual-comb all-fiber mode-locked laser," Photonics Res. **6**(9), 853–857 (2018).
32. Z. Ding, G. Wang, Y. Xiong, *et al.*, "Single-short-cavity dual-comb fiber laser with over 120 kHz repetition rate difference based on polarization multiplexing," Opt. Lett. **48**(20), 5233–5236 (2023).
33. K. Iwakuni, A. Takahashi, and S. Okubo, "Noise characteristics of a polarization-duplex dual-comb fiber laser based on a single gain fiber," Results in Optics **12**, 100476 (2023).
34. B. Rao, M. Li, X. Yang, *et al.*, "Polarization-multiplexed dual-comb fiber laser based on an all-polarization-maintaining cavity configuration," Front. Phys. **10**, 1073201 (2022).
35. X. Sun, Y. Zhu, L. Jin, *et al.*, "Polarization-maintaining all-fiber tunable mode-locked laser based on a thermally controlled Lyot filter," Opt. Lett. **47**(19), 4913–4916 (2022).
36. W. Hänsel, H. Hoogland, M. Giunta, *et al.*, "All polarization-maintaining fiber laser architecture for robust femtosecond pulse generation," Appl. Phys. B **123**(1), 41 (2017).
37. Y. Zhou, Y.-X. Ren, J. Shi, *et al.*, "Dynamics of dissipative soliton molecules in a dual-wavelength ultrafast fiber laser," Opt. Express **30**(12), 21931–21942 (2022).
38. R. Liu, D. Zou, S. Niu, *et al.*, "Collision-induced Hopf-type bifurcation reversible transitions in a dual-wavelength femtosecond fiber laser," Opt. Express **31**(2), 1452–1463 (2023).
39. L. E. Nelson, D. J. Jones, K. Tamura, *et al.*, "Ultrashort-pulse fiber ring lasers," Appl. Phys. B **65**(2), 277–294 (1997).
40. L. M. Zhao, D. Y. Tang, X. Wu, *et al.*, "Observation of dip-type sidebands in a soliton fiber laser," Opt. Commun. **283**(2), 340–343 (2010).
41. Y. Du, X. Shu, H. Cao, *et al.*, "Dynamics of dispersive wave and regimes of different kinds of sideband generation in mode-locked soliton fiber lasers," IEEE J. Sel. Top. Quantum Electron. **24**(3), 1–8 (2018).
42. M. N. Islam, C. D. Poole, and J. P. Gordon, "Soliton trapping in birefringent optical fibers," Opt. Lett. **14**(18), 1011–1013 (1989).
43. Curtis R. Menyuk, "Stability of solitons in birefringent optical fibers. I: Equal propagation amplitudes," Opt. Lett. **12**(8), 614–616 (1987).
44. M. N. Islam, C. R. Menyuk, C.-J. Chen, *et al.*, "Chirp mechanisms in soliton-dragging logic gates," Opt. Lett. **16**(4), 214–216 (1991).